Stability and superionicity of NH_4S and NH_4S_2 at extreme conditions

Kang Yang, Jingming Shi [⬭],[*] Wenwen Cui, Jian Hao, and Yinwei Li[†]

Laboratory of Quantum Functional Materials Design and Application, School of Physics and Electronic Engineering,
Jiangsu Normal University, Xuzhou 221116, China

Stable compounds comprising nitrogen, sulfur, and hydrogen elements hold significant promise in hydride superconductors and astrophysical matter. Herein, we utilize a blend of structure prediction techniques and first-principles calculations to comprehensively explore the N–H–S system. We present the discovery of two ionic compounds, NH_4S and NH_4S_2, characterized by similar NH_4 configurations but distinct arrangements of sulfur atoms. As the sulfur content increases, we observe a transition in the bonding pattern of sulfur-sulfur interactions from S_2 dimers to S_4 units. Furthermore, the electron transfer from NH_4 to each S unit escalates from $1.04\ e$ (NH_4S) to $1.24\ e$ (NH_4S_2). Through *ab initio* molecular dynamics simulations, we unveil a sequence of phase transitions encompassing solid, superionic, and liquid phases for both compounds. Notably, the high-pressure and high-temperature phase diagrams reveal that only the superionic phase of NH_4S corresponds to the extreme conditions found in the interior of the Earth. Moreover, the liquid regions of both compounds encompass the isentropic lines of Neptune, Uranus, and Jupiter. These results could provide essential information for understanding the N–H–S system at high pressure and the formation models of the planets.

I. INTRODUCTION

The application of pressure provides a potent avenue for exploring uncharted phase space and uncovering intricate structures, as it can significantly reduce interatomic distances and reorder the energies of outer atomic orbitals [1,2]. Through the elucidation of compound formation, construction of phase diagrams, and scrutiny of exotic properties, these compounds play pivotal roles in various fields, including superconductors [3–7], high-energy density materials [8–10], photovoltaic materials [11], as well as exhibiting the adiabatic property [12] and exotic matter states relevant to astrophysical objects [13–23]. Consequently, high-pressure compounds showcasing phenomena and applications have garnered considerable attention in condensed matter physics.

The N–H–S system remains a focal point of research due to its distinct physical and chemical behaviors (such as superconducting [24] and planetary mineral [25,26]), coupled with its abundance in interiors of planets [27,28]. Researchers investigate the N–H–S system primarily to search for high-temperature superconducting materials. Notably, the discovery of high-T_c superconductors has been achieved in the H–S binary system [29,30], inspiring subsequent investigations into systems such as La–H [4,31] and Hf–H [32,33], consistently pushing the boundaries of superconducting transition temperatures [34,35]. Li *et al.* [24] investigated the pseudobinary system H_2S–NH_3, demonstrating diverse electrical properties and predicting several stable phases as potential superconductors with T_c up to 50 K. On the other

hand, investigations into the N–H–S system aim mainly to elucidate models of planetary composition and astronomical phenomena. Within the N–H binary system, NH_3, a traditional component of icy matter, has garnered attention for its behavior under high pressure and temperature. Authors of early studies identified an ionic crystal comprising $(NH_2)^-$ and $(NH_4)^+$ under pressure [36]. Subsequent researchers even detected proton diffusion in hot dense ammonia through experimental and *ab initio* molecular dynamics (AIMD) simulations, suggesting the presence of NH_3 within planets [37]. Furthermore, researchers have indicated the presence of potential chromophoric compounds in the N–H–S system, which typically exhibit vibrant colors [25]. NH_4SH and $(NH_4)_2S$ have been proposed as constituents of chromophores [26], given that N, S, and H are primary elements in known chromophores. However, current research data on the stable structures, stoichiometry, and phase diagrams of the N–H–S system under high temperature and high pressure conditions are still insufficient. Thus, investigating the structure and stable stoichiometries of the ternary N–H–S system under high pressure remains a pressing topic in both condensed matter physics and astrophysics.

In this paper, we systematically investigate the phase stability of ternary N–H–S systems under high-pressure and high-temperature (HPHT) conditions. We propose that two polysulfides, NH_4S and NH_4S_2, become energetically stable at pressures exceeding 3 GPa. Further calculations show that, with the increase in sulfur content, the bonding mode of sulfur-sulfur interactions transitions from S_2 dimers to S_4 units. Additionally, the electron transfer from NH_4 to each S unit increases from $1.04\ e$ in NH_4S to $1.24\ e$ in NH_4S_2. AIMD simulations demonstrate that temperature induces transitions from solid state to superionic state and ultimately to liquid

[*]Contact author: jingmingshi@jsnu.edu.cn
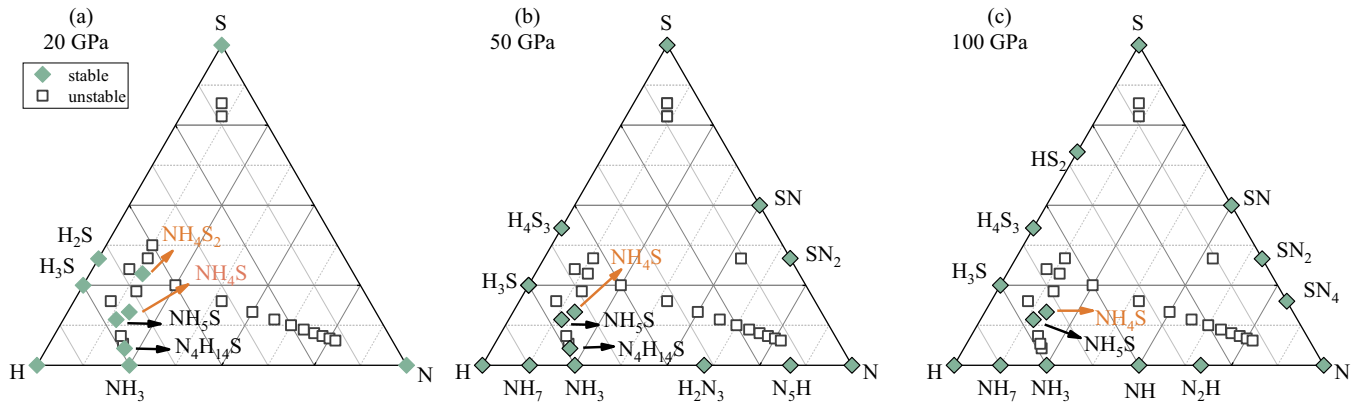[†]Contact author: yinwei_li@jsnu.edu.cn

FIG. 1. The ternary phase diagram of N–H–S at (a) 20 GPa, (b) 50 GPa, and (c) 100 GPa. The cyan rhombuses in the phase diagrams represent thermodynamically stable phases, while the open squares indicate thermodynamically unstable phases. The points indicated by brown arrows represent the stable compounds proposed in this paper, while the points indicated by black arrows represent the stable compounds proposed in previous work.

phases. These findings provide reliable theoretical information for understanding the structure, electronic properties, and dynamic properties of the N–H–S system at high pressure.

II. METHODS

Extensive structure searches on various compositions in the N–H–S system were performed at 20, 50, 100, and 150 GPa. Crystalline structures employ structural prediction up to 4 f.u. using the particle-swarm optimization algorithm (CALYPSO) [38–41]. CALYPSO is one of the most efficient methods for structural prediction and has successfully predicted stable or metastable ground-state structures for various systems at high pressure [4,5,29,42,43]. The following structure relaxations and electronic properties are calculated using density functional theory implemented in VASP code [44,45]. The exchange-correlation potential is adopted with the generalized gradient approximation (GGA) [45] in the form of the Perdew-Burke-Ernzerhof (PBE) [46] functional. Projector augmented-wave pseudopotentials with valence electrons of $2s^2 2p^3$, $1s^1$, and $3s^2 3p^4$ were chosen for N, H, and S, respectively. The Monkhorst-Pack k points with a grid density of $2\pi \times 0.02$ Å^{-1} were chosen to make a total energy convergence of better than 1 meV per atom. The cutoff energy for the expansion of the wave function in the plane-wave basis was set to 1000 eV. The phonon calculations were performed for all structures by using a supercell method as implemented in PHONOPY code [47]. AIMD molecular dynamical simulations were performed in the canonical (NVT) ensemble applying a Nosé-Hoover thermostat [48] combined with a supercell method (288 atoms for NH$_4$S and 224 atoms for NH$_4$S$_2$) with only the Γ point for the Brillouin zone sampling to determine the dynamical properties at high temperatures. Each simulation consists of 10 000 time steps with a time step of 1 fs. The crystal structures and electron localization function (ELF) were plotted using VESTA software [49].

III. RESULTS AND DISCUSSIONS

The formation enthalpies of the predicted N–H–S stoichiometries with respect to the decompositions at selected

pressures are summarized in the Fig. 1. The cyan rhombuses in the phase diagrams represent thermodynamically stable phases, while the open squares indicate thermodynamically unstable phases. At 20 GPa, in addition to previous proposed NH$_5$S and N$_4$H$_{14}$S, we predict two unconventional stoichiometries of the N–H–S system, NH$_4$S and NH$_4$S$_2$, which are energetically stable [Fig. 1(a)]. As the pressure increases to 50 GPa, NH$_4$S$_2$ becomes unstable, while NH$_4$S remains stable and retains its stability up to 100 GPa. The formation enthalpies of all the compositions are calculated at 150 GPa and reveal no stable compounds under this condition. The stable pressure ranges are determined by calculating the enthalpy differences of the predicted stoichiometries relative to all possible decomposition pathways, including all stable phases of the elemental; binary N–H, S–H, and S–N systems; as well as the N–S–H systems, as a function of pressure. The results are summarized in Fig. 2(a). We determined the structural phase transition sequences of previous proposed compositions (NH$_5$S, N$_2$H$_8$S$_5$, NH$_7$S$_2$, N$_2$H$_8$S, and N$_4$H$_{14}$S), which are in good agreement with previous studies [24]. Regarding the other compounds, NH$_4$S remains stable in the *Pba*2 crystal over a wide range from 3 to 116 GPa, and NH$_4$S$_2$ exhibits stability between 3 and 26 GPa in a form of the *Cc* phase. Discussions will be focused on NH$_4$S and NH$_4$S$_2$ because they are unreported stoichiometries.

*Pba*2-NH$_4$S consists of alternating layers of ionic NH$_4$ and S$_2$ dimers [Fig. 2(b)], where the NH$_4$ unit is commonly found in several phases of NH$_3$ [50] and NH$_3$-He compounds [18,23], and the S$_2$ dimer is a prevalent configuration in sulfides such as La-S [51] and Ba-S [52] systems, and they play an important role in the stability of the structure. In the sulfur layers, each S$_2$ dimer has a bond length of 2.11 Å at 50 GPa and does not change when the pressure varies (Fig. S1 in the Supplemental Material (SM) [53]), where the presence of covalent bonding is clearly evidenced by the ELF at this pressure, as shown in Fig. S2 in the SM [53]. Within the NH$_4$ layers, the N–H bond lengths remain ~1.04 Å as pressure increases from 20 to 100 GPa (Fig. S1 in the SM [53]), resembling the covalent N–H bond length (1.01 Å) in NH$_3$ at 50 GPa. Interestingly, the NH$_4$ unit remains stable at a significantly lower pressure of 3 GPa, in contrast with 50 GPa in
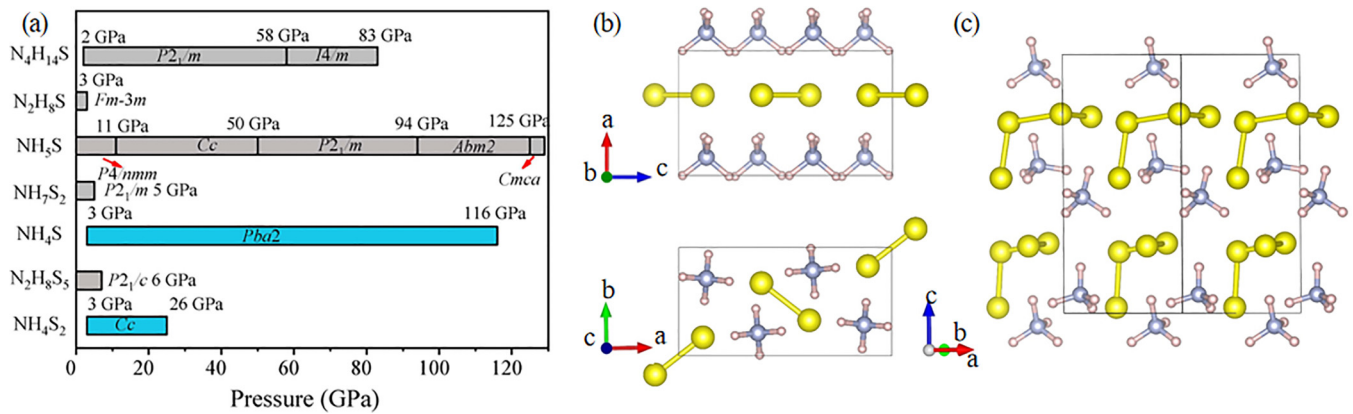
FIG. 2. (a) Phase diagram under high pressure. Colored bars indicate stability of predicted unconventional compounds. Gray bars show the known compounds investigated in a previous study. (b) and (c) Structural configurations of $Pba2$-NH₄S and Cc-NH₄S₂. Upper and lower panels of (b) show side and top views. Blue, pink, and yellow spheres represent N, H, and S atoms, respectively.

N–H compounds [50] and >100 GPa in NH₃–He compounds [18,23]. This suggests that the incorporation of sulfur favors the formation and stability of the NH₄ unit. Further Bader charge calculations show that the S₂ dimer in the NH₄S acts as an anion, with each S₂ dimer receiving 1.04 e from NH₄, thereby forming a strong ionic bond that ensures the stability of the structure, as shown in Table S1 in the SM [53]. The absence of negative phonon dispersion in $Pba2$-NH₄S in the pressure range from 0 to 116 GPa indicates its dynamical stability (Fig. S3 in the SM [53]). The electronic band structure and density of states (DOS) indicate that $Pba2$-NH₄S is an indirect semiconductor with band gap of 1.49 eV at 50 GPa (Fig. S5 in the SM [53]). The projected DOS of NH₄ cations and S₂ dimers below the Fermi level shows a similar trend of change, indicating a significant interaction between them.

NH₄S₂ has Cc symmetry and becomes stable at 3 GPa but quickly becomes energetically unfavorable with respect to NH₄S and S at ∼26 GPa. Compared with the $Pba2$-NH₄S structure, Cc-NH₄S₂ exhibits an alternate arrangement of layered structures with identical NH₄ units but a distinct sulfur arrangement [Fig. 2(c)]. The increased sulfur content causes the NH₄ units to shift outward, forming a framework of differentiated NH₄ layers. Meanwhile, the dense structural configuration causes the S₂ dimers to polymerize into S₄ chains for NH₄S₂, with S–S distances varying from 2.04 to 2.06 Å, forming covalent bonds at 20 GPa (Fig. S2 in the SM [53]). The S–S distance in S₄ chains and N–H bond lengths in the NH₄ unit remain at 2.06 and 1.04 Å at higher pressures, as shown in Fig. S1 in the SM [53]. Authors of previous studies have revealed several structural configuration for sulfur in S-containing materials other than S₂ dimers, such as ring S₄ [54] and V-shaped S₃ [52]. However, in Cc-NH₄S₂, there exists a previously unreported chain structure composed of S₄ units. Bader charge analysis shows that each S₄ chain accepts 1.24 e from two NH₄ units in NH₄S₂ (Table S1 in the SM [53]). NH₄S₂ is confirmed to be dynamically stable across the entire pressure range from 3 to 26 GPa, as indicated by the phonon dispersion without imaginary frequencies. However, it becomes unstable below this pressure, as shown in Fig. S4 in the SM [53], indicating that it cannot be quenched to ambient conditions. Further electronic property studies reveal a band gap of 1.16 eV at 20 GPa and a relatively strong interaction

between NH₄ cations and S₄ anions. This is derived from the relatively large charge transfer from NH₄ to S atoms, allowing more S electrons to occupy the valence band and enhancing the S contribution to the DOS in the Brillouin zone (Fig. S5 in the SM [53]). The structural information of the two predicted compounds is summarized in Table S2 in the SM [53].

To ascertain the atomic behavior characteristics of the predicted compounds NH₄S and NH₄S₂ at HPHT, we conducted AIMD over a wide range of pressures and temperatures. The calculated mean square displacements (MSDs) of individual atoms in the compounds at various temperatures are summarized in Fig. 3. It is obvious that the MSDs of N, S, and H atoms in $Pba2$-NH₄S are a horizontal line with their diffusion coefficients of $D^N = D^H = D^S = 0$ at 20.2 GPa and 300 K, indicating that $Pba2$-NH₄S exhibits a solid character at this condition. This can also be confirmed by the atomic trajectories at this condition, as shown in Fig. S6 in the SM [53], which shows that all the atoms of N, S, and H in the $Pba2$-NH₄S structure vibrate around their equilibrium positions. As the temperature increases to 600 K, the MSD of the H atoms in NH₄S exhibits a linear increase trend, indicating the initiation of H-atom diffusion with $D^H = 1.27 \times 10^{-5}$ cm² s⁻¹ at this temperature, while the N and S atoms continue to undergo minor vibrations at their lattice equilibrium positions with $D^N = D^S = 0$ [Fig. 3(b)], suggesting the transition of NH₄S to a superionic state at this temperature. When the temperature rises to 1600 K, the MSDs of all atoms in $Pba2$-NH₄S increase linearly with time [Fig. 3(c)]. However, the MSD of H atoms increases significantly more than N and S atoms, owing to the relatively smaller atomic mass of H than N and S. This indicates that, at this temperature, $Pba2$-NH₄S transforms from the superionic state to the liquid phase, accompanied by diffusion coefficients of $D^H = 6.54 \times 10^{-4}$ cm² s⁻¹, $D^N = D^S = 1.99 \times 10^{-4}$ cm² s⁻¹. In the meantime, we record the radial distribution functions of N–H, N–S, and S–H in predicted compounds shown in Fig. S7 in the SM [53]. The lower amplitude as the temperature increases indicates the distortion of their sublattice. Further analysis reveals that, at ∼1200 K, $Pba2$-NH₄S converts to a superionic phase at 55.6 GPa, and the critical transition temperature from superionic to liquid increases to 2500 K at 63.5 GPa (Fig. S8 in the SM [53]). As the temperature increases, Cc-NH₄S₂
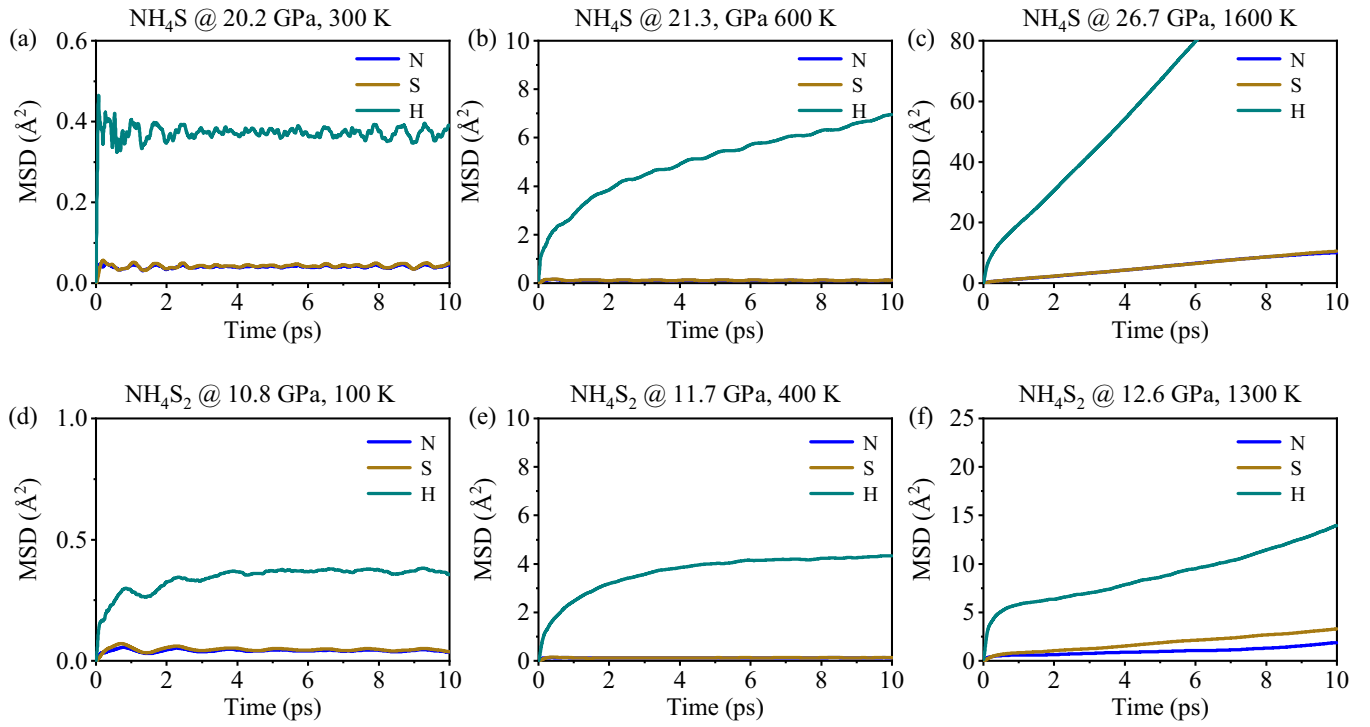
FIG. 3. Atomic behavior in $Pba2$-NH$_4$S and Cc-NH$_4$S$_2$ from *ab initio* molecular dynamics (AIMD) simulations at different pressures and temperatures. (a)–(c) Calculated mean square displacements (MSDs) at 20.2, 21.3, and 26.7 GPa and different temperatures for $Pba2$-NH$_4$S. (d)–(f) MSDs at 10.8, 11.7, and 12.6 GPa and different temperatures for Cc-NH$_4$S$_2$.

will undergo the same phase transition trend as NH$_4$S (solid-superionic-liquid). For example, at ∼10 GPa, Cc-NH$_4$S$_2$ will undergo phase transitions from solid to superionic and from superionic to liquid at 400 and 1300 K, respectively, as shown in Figs. 3(d)–3(f) and Fig. S9 in the SM [53].

Based on the temperature-induced atomic dynamics of NH$_4$S and NH$_4$S$_2$, we have constructed phase diagrams for these compounds under HPHT conditions, as illustrated in Fig. 4. The phase diagrams for both structures are divided

into three regions by two black dashed lines. At relatively lower temperatures, NH$_4$S and NH$_4$S$_2$ exist in the solid phase. With increasing temperature, they transition into a superionic phase. The critical transition temperatures are ∼500 K at 20 GPa and 750 K at 100 GPa for NH$_4$S, which are slightly higher than those for NH$_4$S$_2$ (∼200 K at all pressure ranges). Both compounds exhibit superionic behavior over a significant region of the phase diagram (peach region). At temperatures of 1300 K at 20 GPa and 2500 K at 100 GPa,
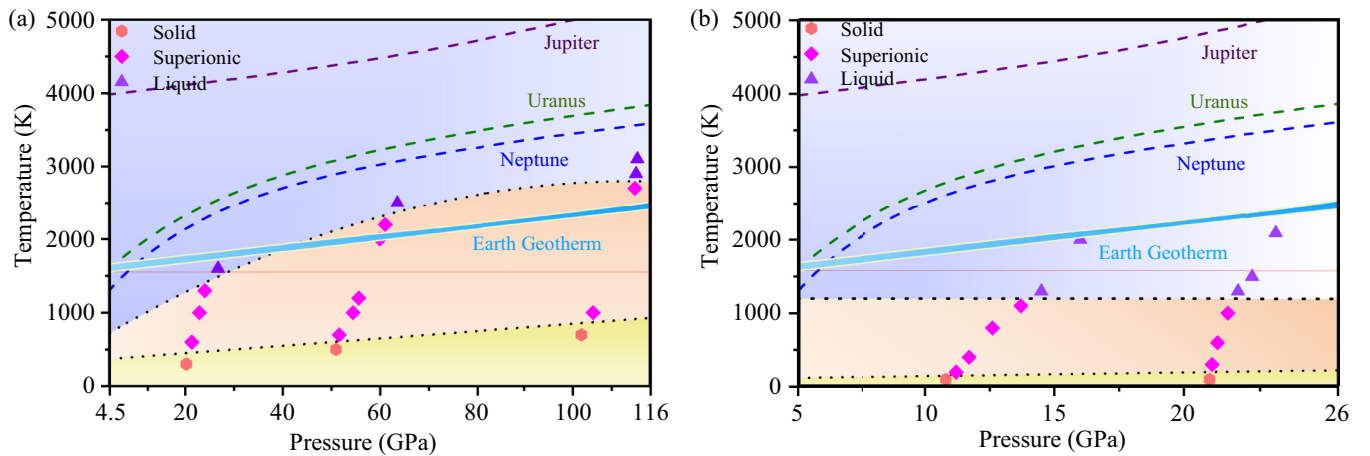

FIG. 4. (a) and (b) Phase diagrams for NH$_4$S and NH$_4$S$_2$ at high pressure and high temperature (HPHT), respectively. yellow, peach, and blue regions represent the solid, superionic, and liquid regions, respectively; red, magenta, and purple points represent solid, superionic, and liquid states, respectively. The thick blue thick line represents the geotherm of the Earth [55]; blue, green, and purple lines represent the isentropic lines of Neptune, Uranus [56], and Jupiter [57], respectively.

NH$_4$S transitions into a liquid phase (light blue region) where all atoms are diffusive. In contrast, NH$_4$S$_2$ transitions to the liquid phase at $\sim$1200 K across all pressure ranges.

By comparing the stability regions of different phases of these compounds with the extreme conditions found in planetary interiors, we observe the geotherm of the Earth across the superionic region of NH$_4$S and the liquid region of NH$_4$S$_2$. This indicates that NH$_4$S might be in a superionic state, while NH$_4$S$_2$ might be in a liquid phase within the interior of the Earth. Given the higher-pressure and temperature conditions in the interiors of Neptune, Uranus, and Jupiter, both NH$_4$S and NH$_4$S$_2$ are expected to exhibit liquid behavior. These findings provide critical insights into the composition and formation models of planets.

IV. CONCLUSIONS

In conclusion, combining structural prediction and first-principles calculations, we identify two unconventional stoichiometries of NH$_4$S and NH$_4$S$_2$ in the N–H–S system that are stable at high pressure. Both compounds consist of ionic NH$_4$ and S units, exhibiting strong ionic character due to the larger electrons transition. The phonon dispersions reveal they are dynamically stable with no imaginary frequency in whole Brillouin zones, and the electronic band structures confirm their semiconductor character. AIMD simulations reveal that the two compounds will follow the state transition of solid-superionic-liquid phases with increasing temperature. The HPHT phase diagram shows that NH$_4$S would be in a superionic state within the interior of the Earth, while both compounds would be in a liquid phase within the interiors of Neptune, Uranus, and Jupiter. These results not only expand the family of N–H–S compounds, but they also contribute to models of the structures and evolution of planetary interiors.

[1] L. Zhang, Y. Wang, J. Lv, and Y. Ma, Materials discovery at high pressures, Nat. Rev. Mater. **2**, 17005 (2017).

[2] M. Xu, Y. Li, and Y. Ma, Materials by design at high pressures, Chem. Sci. **13**, 329 (2022).

[3] A. Drozdov, M. Eremets, I. Troyan, V. Ksenofontov, and S. I. Shylin, Conventional superconductivity at 203 Kelvin at high pressures in the sulfur hydride system, Nature (London) **525**, 73 (2015).

[4] H. Liu, I. I. Naumov, R. Hoffmann, N. Ashcroft, and R. J. Hemley, Potential high-T_c superconducting lanthanum and yttrium hydrides at high pressure, Proc. Natl. Acad. Sci. USA **114**, 6990 (2017).

[5] W. Cui, T. Bi, J. Shi, Y. Li, H. Liu, E. Zurek, and R. J. Hemley, Route to high-T_c superconductivity via CH$_4$-intercalated H$_3$S hydride perovskites, Phys. Rev. B **101**, 134504 (2020).

[6] Y. Sun, Y. Tian, B. Jiang, X. Li, H. Li, T. Iitaka, X. Zhong, and Y. Xie, Computational discovery of a dynamically stable cubic SH$_3$-like high-temperature superconductor at 100 GPa via CH$_4$ intercalation, Phys. Rev. B **101**, 174102 (2020).

[7] X. Song, X. Hao, X. Wei, X.-L. He, H. Liu, L. Ma, G. Liu, H. Wang, J. Niu, S. Wang *et al.*, Superconductivity above 105 K in nonclathrate ternary lanthanum borohydride below megabar pressure, J. Am. Chem. Soc. **146**, 13797 (2024).

[8] Y. Li, J. Hao, H. Liu, S. Lu, and J. S. Tse, High-energy density and superhard nitrogen-rich B-N compounds, Phys. Rev. Lett. **115**, 105502 (2015).

[9] K. Yang, J. Shi, W. Cui, J. Hao, and Y. Li, Prediction of a reservoir of N-rich high-energy density material at the Earth's mantle, Phys. Chem. Chem. Phys. **25**, 20281 (2023).

[10] F. Peng, Y. Ma, A. Hermann, and M. Miao, Recoverable high-energy compounds by reacting methane and nitrogen under high pressure, Phys. Rev. Mater. **4**, 103610 (2020).

[11] S. Ding, J. Shi, J. Xie, W. Cui, P. Zhang, K. Yang, J. Hao, L. Zhang, and Y. Li, Helium incorporation induced direct-gap silicides, npj Comput. Mater. **7**, 89 (2021).

[12] A. S. Naumova, S. V. Lepeshkin, P. V. Bushlanov, and A. R. Oganov, Unusual chemistry of the C–H–N–O system under pressure and implications for giant planets, J. Phys. Chem. A **125**, 3936 (2021).

[13] P. Huang, H. Liu, J. Lv, Q. Li, C. Long, Y. Wang, C. Chen, R. J. Hemley, and Y. Ma, Stability of H$_3$O at extreme conditions and implications for the magnetic fields of Uranus and Neptune, Proc. Natl. Acad. Sci. USA **117**, 5638 (2020).

[14] H. Gao, C. Liu, J. Shi, S. Pan, T. Huang, X. Lu, H.-T. Wang, D. Xing, and J. Sun, Superionic silica-water and silica-hydrogen compounds in the deep interiors of Uranus and Neptune, Phys. Rev. Lett. **128**, 035702 (2022).

[15] S. Pan, T. Huang, A. Vazan, Z. Liang, C. Liu, J. Wang, C. J. Pickard, H.-T. Wang, D. Xing, and J. Sun, Magnesium oxide-water compounds at megabar pressure and implications on planetary interiors, Nat. Commun. **14**, 1165 (2023).

[16] L. Zhu, H. Liu, C. J. Pickard, G. Zou, and Y. Ma, Reactions of xenon with iron and nickel are predicted in the Earth's inner core, Nat. Chem. **6**, 644 (2014).

[17] J. Zhang, H. Liu, Y. Ma, and C. Chen, Direct H-He chemical association in superionic FeO$_2$H$_2$He at deep-Earth conditions, Natl. Sci. Rev. **9**, nwab168 (2022).

[18] J. Shi, W. Cui, J. Hao, M. Xu, X. Wang, and Y. Li, Formation of ammonia-helium compounds at high pressure, Nat. Commun. **11**, 3164 (2020).

[19] P. Zhang, J. Shi, W. Cui, C. Liu, S. Ding, K. Yang, J. Hao, and Y. Li, Formation of NH$_3$-Xe compound at the extreme condition of planetary interiors, Phys. Rev. B **105**, 214109 (2022).

[20] S. Ding, P. Zhang, K. Yang, C. Liu, J. Hao, W. Cui, J. Shi, and Y. Li, Formation of solid SiO_2He compound at high pressure and high temperature, Phys. Rev. B **106**, 024102 (2022).

[21] C. Liu, J. Wang, X. Deng, X. Wang, C. J. Pickard, R. Helled, Z. Wu, H.-T. Wang, D. Xing, and J. Sun, Partially diffusive helium-silica compound under high pressure, Chin. Phys. Lett. **39**, 076101 (2022).

[22] M. Zou, K. Yang, P. Zhang, W. Cui, J. Hao, J. Shi, and Y. Li, Existence of solid Na–Xe compounds at the extreme conditions of Earth's interior, Phys. Rev. Res. **5**, 043107 (2023).

[23] C. Liu, H. Gao, A. Hermann, Y. Wang, M. Miao, C. J. Pickard, R. J. Needs, H.-T. Wang, D. Xing, and J. Sun, Plastic and superionic helium ammonia compounds under high pressure and high temperature, Phys. Rev. X **10**, 021007 (2020).

[24] X. Li, A. Lowe, L. Conway, M. Miao, and A. Hermann, First principles study of dense and metallic nitric sulfur hydrides, Commun. Chem. **4**, 83 (2021).

[25] C. Sagan, E. R. Lippincott, M. O. Dayhoff, and R. Eck, Organic molecules and the coloration of Jupiter, Nature (London) **213**, 273 (1967).

[26] K. I. Ibragimov and A. Solodovnik, Ammonia hydrosulphide and cloudiness in the atmospheres of the giant planets, Kinemat. Fiz. Nebesnyh Tel **7**, 58 (1991).

[27] B. Marty, T. Guillot, A. Coustenis, the Kronos consortium, N. Achilleos, Y. Alibert, S. Asmar, D. Atkinson, S. Atreya, G. Babasides *et al.*, Kronos: Exploring the depths of Saturn with probes and remote sensing through an international mission, Exp. Astron. **23**, 947 (2009).

[28] O. Mousis, D. H. Atkinson, R. Ambrosi, S. Atreya, D. Banfield, S. Barabash, M. Blanc, T. Cavalié, A. Coustenis, M. Deleuil *et al.*, *In situ* exploration of the giant planets, Exp. Astro. **54**, 975 (2022).

[29] Y. Li, J. Hao, H. Liu, Y. Li, and Y. Ma, The metallization and superconductivity of dense hydrogen sulfide, J. Chem. Phys. **140**, 174712 (2014).

[30] D. Duan, Y. Liu, F. Tian, D. Li, X. Huang, Z. Zhao, H. Yu, B. Liu, W. Tian, and T. Cui, Pressure-induced metallization of dense $(H_2S)_2H_2$ with high-T_c superconductivity, Sci. Rep. **4**, 6968 (2014).

[31] A. Drozdov, P. Kong, V. Minkov, S. Besedin, M. Kuzovnikov, S. Mozaffari, L. Balicas, F. Balakirev, D. Graf, V. Prakapenka *et al.*, Superconductivity at 250 K in lanthanum hydride under high pressures, Nature (London) **569**, 528 (2019).

[32] K. Gao, W. Cui, J. Chen, Q. Wang, J. Hao, J. Shi, C. Liu, S. Botti, M. A. L. Marques, and Y. Li, Superconducting hydrogen tubes in hafnium hydrides at high pressure, Phys. Rev. B **104**, 214511 (2021).

[33] H. Xie, Y. Yao, X. Feng, D. Duan, H. Song, Z. Zhang, S. Jiang, S. A. T. Redfern, V. Z. Kresin, C. J. Pickard *et al.*, Hydrogen pentagraphenelike structure stabilized by hafnium: A high-temperature conventional superconductor, Phys. Rev. Lett. **125**, 217001 (2020).

[34] G. Gao, L. Wang, M. Li, J. Zhang, R. T. Howie, E. Gregoryanz, V. V. Struzhkin, L. Wang, and J. S. Tse, Superconducting binary hydrides: Theoretical predictions and experimental progresses, Mater. Today Phys. **21**, 100546 (2021).

[35] X. Wei, X. Hao, A. Bergara, E. Zurek, X. Liang, L. Wang, X. Song, P. Li, L. Wang, G. Gao *et al.*, Designing ternary superconducting hydrides with A15-type structure at moderate pressures, Mater. Today Phys. **34**, 101086 (2023).

[36] C. J. Pickard and R. Needs, Highly compressed ammonia forms an ionic crystal, Nat. Mater. **7**, 775 (2008).

[37] S. Ninet, F. Datchi, and A. M. Saitta, Proton disorder and superionicity in hot dense ammonia ice, Phys. Rev. Lett. **108**, 165702 (2012).

[38] Y. Wang, J. Lv, L. Zhu, and Y. Ma, Crystal structure prediction via particle-swarm optimization, Phys. Rev. B **82**, 094116 (2010).

[39] Y. Wang, J. Lv, L. Zhu, and Y. Ma, CALYPSO: A method for crystal structure prediction, Comput. Phys. Commun. **183**, 2063 (2012).

[40] B. Gao, P. Gao, S. Lu, J. Lv, Y. Wang, and Y. Ma, Interface structure prediction via CALYPSO method, Sci. Bull. **64**, 301 (2019).

[41] X. Shao, J. Lv, P. Liu, S. Shao, P. Gao, H. Liu, Y. Wang, and Y. Ma, A symmetry-orientated divide-and-conquer method for crystal structure prediction, J. Chem. Phys. **156**, 014105 (2022).

[42] F. Peng, Y. Sun, C. J. Pickard, R. J. Needs, Q. Wu, and Y. Ma, Hydrogen clathrate structures in rare earth hydrides at high pressures: Possible route to room-temperature superconductivity, Phys. Rev. Lett. **119**, 107001 (2017).

[43] X. Liang, X. Wei, E. Zurek, A. Bergara, P. Li, G. Gao, and Y. Tian, Design of high-temperature superconductors at moderate pressures by alloying AlH_3 or GaH_3, Matter Radiat. Extremes **9**, 018401 (2024).

[44] G. Kresse and J. Furthmüller, Efficient iterative schemes for *ab initio* total-energy calculations using a plane-wave basis set, Phys. Rev. B **54**, 11169 (1996).

[45] J. P. Perdew, K. Burke, and M. Ernzerhof, Generalized gradient approximation made simple, Phys. Rev. Lett. **77**, 3865 (1996).

[46] P. E. Blöchl, O. Jepsen, and O. K. Andersen, Improved tetrahedron method for Brillouin-zone integrations, Phys. Rev. B **49**, 16223 (1994).

[47] A. Togo, F. Oba, and I. Tanaka, First-principles calculations of the ferroelastic transition between rutile-type and $CaCl_2$-type SiO_2 at high pressures, Phys. Rev. B **78**, 134106 (2008).

[48] W. G. Hoover, Canonical dynamics: Equilibrium phase-space distributions, Phys. Rev. A **31**, 1695 (1985).

[49] K. Momma and F. Izumi, VESTA3 for three-dimensional visualization of crystal, volumetric and morphology data, J. Appl. Crystallogr. **44**, 1272 (2011).

[50] G.-R. Qian, H. Niu, C.-H. Hu, A. R. Oganov, Q. Zeng, and H.-Y. Zhou, Diverse chemistry of stable hydronitrogens, and implications for planetary and materials sciences, Sci. Rep. **6**, 25947 (2016).

[51] K. Gao, W. Cui, Q. Wang, J. Hao, J. Shi, S. Botti, M. A. L. Marques, and Y. Li, Superconductivity in S-rich phases of lanthanum sulfide under high pressure, Phys. Rev. Mater. **6**, 064801 (2022).

[52] S. Wang, S. Liu, P. Gao, J. Lv, Y. Wang, and G. Yang, Semiconducting BaS_3 phase featuring v-shape S_3 unit at high pressure, Phys. Rev. Res. **4**, 023046 (2022).

[53] See Supplemental Material at http://link.aps.org/supplemental/10.1103/PhysRevB.110.054111 for ELF, phonon dispersions, electronic band structures, DOS, structural parameters, Bader charge transformation, MSD, RDF, and atomic trajectories.

[54] M. W. Wong and R. Steudel, Structure and spectra of tetrasulfur S$_4$—An *ab initio* MO study, Chem. Phys. Lett. **379**, 162 (2003).

[55] T. Katsura, A. Yoneda, D. Yamazaki, T. Yoshino, and E. Ito, Adiabatic temperature profile in the mantle, Phys. Earth Planet. Inter. **183**, 212 (2010).

[56] R. Redmer, T. R. Mattsson, N. Nettelmann, and M. French, The phase diagram of water and the magnetic fields of Uranus and Neptune, Icarus **211**, 798 (2011).

[57] W. B. Hubbard and B. Militzer, A preliminary Jupiter model, Astrophys. J. **820**, 80 (2016).